First-principles study of the atomic and electronic structures of crystalline and amorphous B_4C

V. I. Ivashchenko* and V. I. Shevchenko
Institute of Problems of Material Science, NAS of Ukraine, Krzhyzhanosky Str. 3, 03142 Kyiv, Ukraine

P. E. A. Turchi
Lawrence Livermore National Laboratory (L-352), P.O. Box 808, Livermore, California 94551, USA
(Received 2 September 2009; revised manuscript received 13 November 2009; published 31 December 2009)

The atomic and electronic structures of crystalline and amorphous B_4C were determined within density function theory using the local density approximation and a plane-wave pseudopotential method. For the crystalline phases, chain, and polar structures were considered. The structural parameters were obtained by minimizing the total energy with respect to the size, shape, and internal degrees of freedom of 15 and 45-atom unit cells. The amorphous 120 and 135-atom samples of a-B_4C were generated using molecular dynamic simulations in the NVT ensemble using different initial structures. The 120-atom sample was generated from a rhombohedral c-B_4C cell, whereas the a-135 sample was obtained from a fcc B_4C initial structure that differs essentially from the real crystalline B_4C structure. Analysis of the computed results shows that: (i) a random icosahedral network connected with the amorphous B-C matrix is identified in the case of a-B_4C; (ii) carbon clusters are observed in the case of the 120-atom sample of an amorphous matrix; (iii) no chain atoms are found in both amorphous samples that can be explained by their bulk moduli that are lower compared to those of their crystalline counterparts; (iv) the chain and polar B_4C phases transform into a-B_4C under high pressure; and (v) all crystalline structures studied so far are semiconducting, whereas a-B_4C is a semimetal.

DOI: 10.1103/PhysRevB.80.235208 PACS number(s): 77.84.Bw, 74.81.Bd, 61.43.Bn, 61.43.Dq

I. INTRODUCTION

Boron carbide B_4C is an important material that, due to its outstanding hardness, excellent mechanical, thermal, and electrical properties, is widely used for grinding, polishing, surface hardening, and as the main component for producing wear-resistant tools and light-weight armors.[1] Boron carbide is also a known neutron absorber widely used to control the reactivity of nuclear reactors. The local atomic structure of B_4C responsible for these properties is represented by distorted $B_{11}C$ icosahedra located at the nodes of a rhombohedral lattice.[1] This is modification of the α-B_{12} phase that accommodates three-atom chains aligned along the (111) rhombohedral axis linking different $B_{11}C$ icosahedra. According to the accepted classification,[2,3] one can single out three ordered configurations of B_4C: (i) The icosahedra consist of boron atoms, whereas the carbon atoms lie entirely in intericosahedral chains (C-C-C) (chain configuration); (ii) The structure that contains the C-B-C chains and the $B_{11}C$ icosahedra, where carbon atoms occupy polar sites forming bonds with the neighboring icosahedra (polar configuration); and (iii) The equatorial configuration that is similar to the polar one, except that the carbon atoms in the $B_{11}C$ icosahedra occupy equatorial sites forming bonds with the linear chains. Although all these configurations can be realized and assisted by substitutional disorder, the polar configuration is predominant in agreement with x-ray diffraction data.[4,5]

Crystalline boron carbide can be transformed into amorphous by: neutron and He^+ irradiations,[6] shock loading,[7] nanoindentation and scratch test,[8–12] electric field,[13] and depressurization from high pressure.[14] The structure changes of B_4C under neutron irradiation were interpreted in the framework of a microscopic model.[6] This model assumes that the C-B-C linear chains are destroyed, and the boron atoms that are eliminated during irradiation are replaced in the icosahedra by other boron and carbon atoms supplied by the linear C-B-C chains. High-resolution electron microscopy observations of recovered B_4C fragments produced by shock loading revealed the formation of 2–3 nm wide zones of amorphous B_4C phase, that is responsible for a loss of shear strength.[7] Theoretical analysis revealed that such a failure of B_4C was commensurate with the segregation of boron icosahedra embedded in amorphous carbon in 2–3 nm-wide amorphous bands along the (133) crystallographic plane.[15] Similar structures were obtained under quasistatic conditions, using nanoindentation or scratch test.[8–12] The application of an electric field to B_4C induced transformations that are comparable with those obtained under shock or nanoindentation.[13] In Ref. 14, it was reported that the amorphization of boron carbide in the form of nanosized bands took place during unloading from high pressures, and nonhydrostatic stresses played a critical role in the high-pressure amorphization. The investigations of Raman spectra showed that, in comparison with the spectrum of pristine B_4C, the most notable feature in the Raman spectra from amorphous samples was the appearance of two new bands: a high-intense band at 1320–1360 cm^{-1} and with a shoulder peak at 1500–1600 cm^{-1}, and a small peak at 1870–1830 cm^{-1}.[8–13] The two first bands are identified as D and G modes, respectively. The G mode in the range of 1500–1600 cm^{-1} is known from the stretching vibration of sp^2 carbon, whether in C=C chains or in aromatic rings, whereas the D mode in the range of 1260–1420 cm^{-1} is attributed to the breathing modes of the sp^2 carbon aromatic rings.[16,17] The origin of the high-frequency peak at ~1800 cm^{-1} was not fully understood, although this peak was assigned to the stretching of the carbon-boron sp^3 double bonding between carbon aromatic rings.[10]

Amorphous boron carbide films prepared by plasma chemical-vapor deposition,[18] ion beam sputtering,[19] and

magnetron sputtering[20,21] have an amorphous network that differs from that of the bulk a-B_4C samples considered above. According to the results presented in Refs. 18 and 19, the structure of a-B_4C is based on a random icosahedral network, with the boron atoms having two different chemical environments associated with the $B_{11}C$ icosahedral unit and the C-B-C chains connecting the icosahedra. In the amorphous films, the number of chain atoms strongly decreased as the deposition temperature increased from 100 to 600 °C.[19] The chains were absent in as-deposited amorphous B_4C films.[20,21] Also, the carbon clustering was not observed in all amorphous films. The amorphous structure of the films was found to be very similar to that of the irradiated B_4C.[6] Both the bulk and film a-B_4C demonstrate weak mechanical characteristics as compared to their crystalline counterparts.[10,21]

The atomic configurations and bulk moduli of the chain, polar, and equatorial B_4C were investigated in the framework of a first-principles pseudopotential approach (PP).[3] For this purpose, 15-atom rhombohedral computational cells were considered. Similar calculations were carried out for 45-atom hexagonal polar and chain cells.[22,23] So far as we know theoretical investigations of the atomic and electronic structures of a-B_4C are lacking. Hence, atomistic modeling of this amorphous material is highly desirable to gain insight into the mechanisms of structural changes during amorphous-phase formation.

In this work, we study the atomic and electronic structures of the crystalline and amorphous phases of B_4C using a first-principles PP molecular dynamics (MD) technique. The polar and chain crystalline phases as well two amorphous structures of B_4C were considered to simulate the crystalline and amorphous structures of B_4C mentioned above. In particular, we showed above that the amorphous structure of the bulk samples derived from crystalline counterparts differed from that of films and irradiated materials. We will assume that, in the first case, the amorphous phases inherit some of the features of the crystalline counterparts, whereas in the second case the film amorphous structure is formed from a condensation of a boron-carbon gas mixture. Under high irradiation dose, the damage of a B_4C crystal becomes so strong that the final amorphous structure does not have common features with the structure of an initial crystal. We considered the rhombohedral polar supercell and the fcc (face-centered cubic) supercell as initial configurations for MD simulations of the two kinds of amorphous B_4C structures discussed above. Our motivation was that the final a-B_4C would be originated from c-B_4C in the first case, and from the cubic structure (that does not have common features with the rhombohedral chain structure) in the second case, to mimic the structure of amorphous films and neutron-irradiated bulk materials.

The paper is organized as follows. Sec. II contains the details of the computational procedure. In Secs. III A and III B, the computed atomic configurations of the crystalline and amorphous B_4C are presented and discussed. The effect of the structure on the hardness of boron carbide is analyzed. Sec. III C, is devoted to an analysis of the pressure-induced phase transition in c-B_4C and a-B_4C. The densities of states of the crystalline and amorphous phases are studied in Sec. III D. Finally, in Sec. IV the main conclusions are presented.

II. COMPUTATIONAL DETAILS

A first-principles PP procedure was employed to investigate the crystalline, liquid, and amorphous structures of B_4C. Scalar-relativistic band-structure calculations within the local-density approximation (LDA) of density functional theory (DFT) were carried out for 15-atom rhombohedral cells with chain (CHE-15) and polar (POL-15) arrangements of atoms. Also, the 45-atom hexagonal supercells that represent the superposition of three rhombohedral cells were considered (CHE-45 and POL-45). The calculations were also carried out for two forms of pure boron structures, namely the 12-atom rhombohedral phase (BOR-12) and the 36-atom hexagonal phase (BOR-36). The Quantum-ESPRESSO first-principles code[24] was used to perform the PP calculations with norm-conserving PP generated according to the von Barth-Car scheme[24] to describe the electron-ion interaction. Plane waves up to a kinetic energy cutoff of 36 Ry were included in the basis set. The exchange-correlation energy and potential used to implement the LDA are those determined by Ceperley and Alder,[25] as interpolated by Perdew and Zunger.[26] Brillouin-zone (BZ) integrations have been performed using sets of special points corresponding to the (333) Monkhorst-Park shifted mesh.[27] Each eigenvalue was convoluted with a Gaussian with the width $\sigma=0.02$ Ry. The simultaneous relaxation of the ions and the unit cell without the preservation of cell symmetry were carried out in the framework of the Parrinello-Rahman approach[28] that was available in the computer code.[24] The relaxation of the atomic coordinates and unit cell was considered to be complete when the atomic forces were less than 1.0 mRy/bohr, the stresses were smaller than 10 MPa, and the total energy during the structural-optimization iterative process was changing by less than 0.1 mRy.

MD simulations of the liquid and amorphous B_4C phases were carried out with a 135-atom cubic cell and a 120-atom rhombohedral cell using the NVT (the constant number of particles-volume-temperature) ensemble. For this purpose we used the first-principles MD code that was part of the Quantum ESPRESSO software.[24] The initial 135-atom structures (l-135, a-135) represent the (222) fcc supercell, whereas the initial 120-atom structures (l-120, a-120) were generated on the basis of the (222) rhombohedral supercell. For these structures, the macroscopic densities were fixed at the calculated density for the POL-15 crystalline structure. The initial structures were heated up to 4500 K and then equilibrated for 1.0 ps. The systems showed a diffusive behavior and were therefore characterized as liquids. The liquids were cooled down to 300 K for 5.0 ps and again equilibrated for 1.0 ps. The time step was 20 a.u. MD simulations were carried out using the energy cutoff of 24 Ry and only the Γ point was taken into account in the BZ integration. The final samples were relaxed relative to the cell volume and the atomic positions without the preservation of cell symmetry. In this case, the energy cut-off was 36 Ry, and the (222) Monkhorst-Park shifted mesh was used in the BZ integration.

The calculations of the bulk modulus B and its pressure derivative were achieved by changing the cell volume of the computed structures about their equilibrium geometry, and

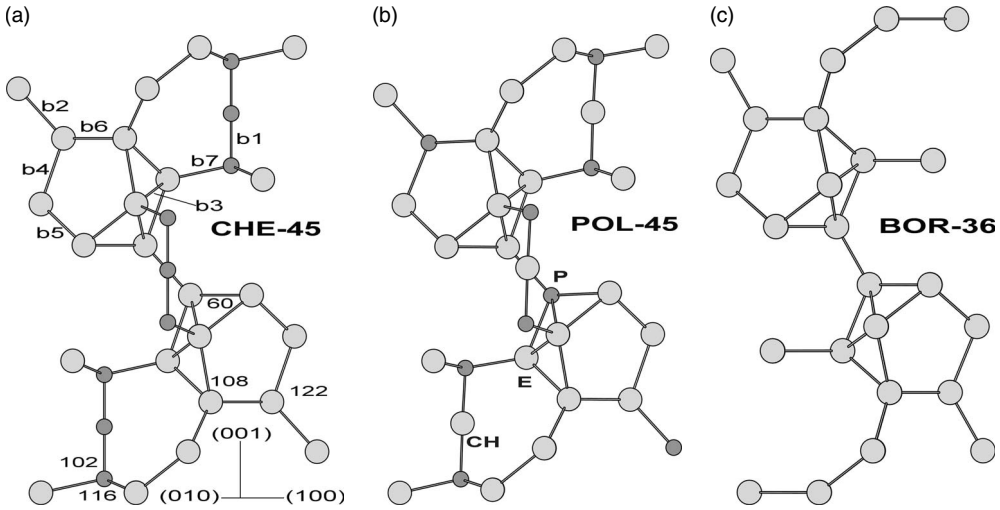

FIG. 1. Atomic configurations inside the hexagonal unit cells of B_4C aligned along the *c*-axis (001). Notations: b_1-b_7—characteristic bond lengths; CH, P, E—atomic positions in the chain, polar and equatorial surroundings, respectively; numbers—characteristic bond angles.

fitting the energy-volume data to a Murnaghan equation of states. The density of states of c-B_4C and a-B_4C was calculated with a tetrahedron method[24] using the (666) and (222) Monkhorst-Park non-shifted meshes, respectively.

III. RESULTS AND DISCUSSION

A. Structural properties of c-B_4C

In this section, we investigate the character of the structural relaxation in the crystalline phases since this question was still not fully addressed in past works.[3,22,23] It was shown that, among three possible configurations of carbon atoms in a rhombohedral cell (equatorial, chain, and polar), the structure with the polar configuration had the lowest total energy, whereas the chain model had the highest-total energy.[3] We will focus below on two latter structures. We have found that the polar phase had an energy gain of 0.0725 eV/atom compared to the chain phase, which was in good agreement with the corresponding value of 0.073 eV/atom obtained for a 15-atom structure in Ref. 3. In Fig. 1 we show the atomic arrangements inside the hexagonal unit cells of the 45 and 36-atom crystalline structures obtained after structural optimization. The structural parameters of all the calculated phases are summarized in Tables I and II. In the case of the 15-atom models, the CHE-15 structure has the rhombohedral $R\bar{3}m$ symmetry, whereas the POL-15 phase

TABLE I. Lattice parameters (a, b, c; α, β, γ) and bulk modulus (B) of the c-B_4C, and a-B_4C phases. Notation: R, H—rhombohedral and hexagonal phases, respectively; N—a number of atoms in a unt cell.

Structure	N	Lattice parameters a, b, c (Å)/α, β, γ (°)	Lattice parameters a, b, c (Å)/α, β, γ (°)	B (GPa)	B (GPa)
CHE	15	5.121/65.98 (R)	5.12/65.9 (R)[a]	270	
	45	5.577, 11.947 (H)	5.577, 11.969 (H)[b]	270	241[b]
POL	15	5.010, 5.143, 5.143/ 65.57, 66.39, 66.39	5.10/65.8 (R)[a] 5.155/65.679 (R)[c]	271	248[a]
	45	5.548, 5.548, 11.865/ 91.74, 88.26, 119.89	5.697, 11.604 (H)[b] 5.60, 12.09 (H)[d]	270	229[b] 241[f]
BOR	12	4.899/58.4 (R)		258	
	36	4.838, 12.295 (H)	4.927, 12.564 (H)[e]	258	
a-B_4C	135	9.849, 9.735, 9.858/90, 90 90		259	
a-B_4C	120	10.104, 10.182, 10.050/ 64.88, 65.24, 66.73		266	

[a](LDA-PP) Ref. 3.
[b](LDA-PP) Ref. 23.
[c](Neutron diffraction) Ref. 29.
[d](XRD) Ref. 30.
[e](XRD) Ref. 31.
[f](Experiment) Ref. 32.

TABLE II. Bond lengths (b_j) in Å for CHE-45, POL-45 and BOR-36 samples in comparison with those from other similar theoretical and experimental structures. Notations: Cb—central atom in a chain, Ch—end atom in a chain, P—polar site, E—equatorial site, P1–P2—distance between the polar sites in the neighboring icosahedra (see text).

Bonds		CHE-45	POL-45	BOR-36	CHE-15[a]	POL-15[b]	Expt.[c]	Expt.[d]	Expt.[e]
b1	Cb-Ch	1.33	1.42,1.43		1.30	1.42	1.434	1.438	1.429
b2	P1-P2	1.70	1.66	1.65	1.70	1.71	1.716	1.699	1.732
b3	E-E	1.73	1.73,1.74	1.75	1.73	1.73	1.693	1.687	1.773
b4	P-E	1.77	1.72	1.75	1.77	1.78	1.758	1.760	1.796
b5	P-E	1.77	1.77	1.77	1.77	1.77	1.762	1.761	1.796
b6	P-P	1.80	1.74,180	1.71	1.81	1.78	1.805	1.810	1.821
b7	Ch-E	1.65	1.58,1.61		1.65	1.59	1.675	1.669	1.617

[a](LDA-PP) Ref. 3.
[b](LDA-PP) Ref. 23.
[c](Neutron diffraction) Ref. 29.
[d](XRD) Ref. 30.
[e](XRD) Ref. 31.

has a monoclinic structure that can be derived from the rhombohedral one by introducing a small monoclinic distortion. Here, it should be noted that similar changes in the crystalline structure of B_4C from the chain to the polar configuration were detected in Ref. 3. The CHE-45 structure has a rhombohedral trimolecular unit cell corresponding to a hexagonal cell containing nine molecular units in the location of the space group $R\bar{3}m$. The three C atoms are located along the hexagonal c-axis, as shown in Fig. 1. The substitution of one B atom in an icosahedron induces a small distortion that transforms the hexagonal structure into a triclinic one. The point group of all the boron structures is $R\bar{3}m$.

A comparison of the structural parameters obtained in this work and in other theoretical and experimental studies indicates a reasonable agreement among them (cf. Table I). However, a noticeable difference is observed between the c-parameters: the theoretical values are lower than the experimental ones. The bulk modulus for our structures is found to be higher compared to that obtained in other theoretical and experimental investigations. Such a discrepancy can be attributed to a relatively small value of the energy cutoff of 36 Ry used in our approach compared to the 65 and 64 Ry used in previous PP calculations.[3,22] Here, we note that our results point out that the relaxed 15 and 45-atom polar structures have monoclinic and triclinic symmetry, respectively, instead of the rhombohedral and hexagonal ones. We note also that the monoclinic and triclinic distortions leading to the corresponding symmetry changes are small (cf. Table I). One can see from Table II that our calculated bond lengths agree well with neutron[29] and x-ray[30,31] diffraction data. An agreement is also found between our results and the theoretical data reported in Refs. 3 and 23.

Based on the analysis of the computed structures, we suppose that the polar configuration will be closest to the c-B_4C structures observed in experiment. However, it is worth noting that due to disorder and temperature effects in the real structure of B_4C, carbon atoms will occupy chain, polar and equatorial positions chaotically. As a result, such structures will have higher symmetry than our ordered structures that are considered here.

B. Structural properties of a-B_4C

In Fig. 2, we show the computed pair-correlation function (PCF) of the liquid and amorphous 120- and 135-atom samples of B_4C. The PCFs of the two l-B_4C models are similar and characterized by a smooth band of nearest-neighbor (NN) correlations. In the amorphous samples, this band transforms into a distinct peak caused by the B-B, B-C, and C-C NN correlations. One can note from Fig. 2 that the B-C correlations weaken and the B-B and C-C correlations strengthen when going from a-135 to a-120, which is also confirmed by the percentage of the B-B, B-C and C-C bonds: 65.2, 34.0 and 0.8% for a-135 and 69.2, 27.6 and 3.2% for a-120, respectively. In both amorphous samples, the second NN correlations are weakly noticeable and centered around 2.9 Å.

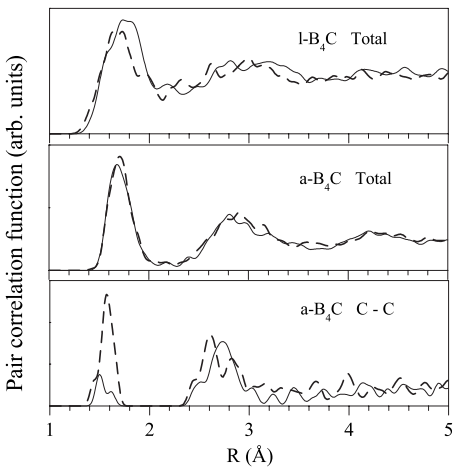

FIG. 2. Computed pair-correlation functions of liquid and amorphous B_4C (l-B_4C and a-B_4C, respectively) represented by 120-atom (dashed line) and 135-atom (solid line) supercells.

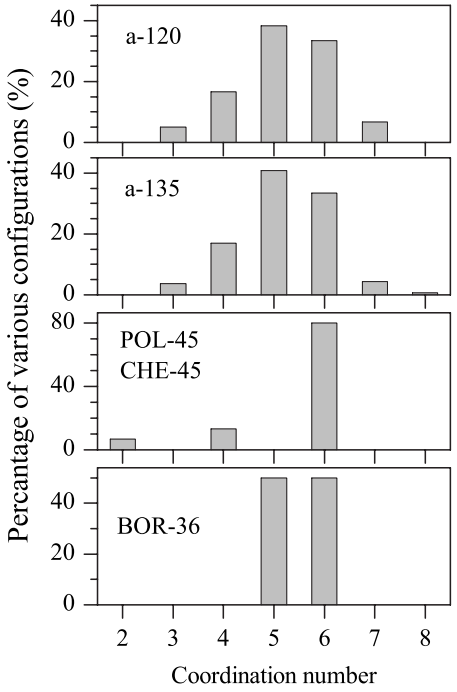

FIG. 3. Percentage of various coordination numbers in amorphous and crystalline B_4C.

The distribution of the atoms with different surroundings in the crystalline and amorphous samples is presented in Fig. 3. Both amorphous samples show similar distributions. The absence of the eightfold coordinated atoms in the a-120 sample indicates that its amorphous network is less random as compared to that of the a-135 sample. Furthermore, the number of threefold coordinated atoms in the first sample is higher than in the second one. These threefold coordinated atoms are absent in the crystalline structures. On the other hand, the twofold coordinated chain atoms, which are characteristic of c-B_4C, are missing in both amorphous phases. Naturally, in the absence of chain atoms, the BOR-36 sample has only five and sixfold coordinated atoms that are shared.

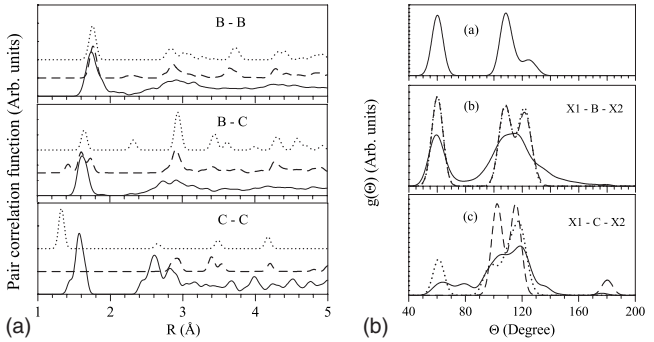

FIG. 5. (Left) Pair correlation functions for the a-120 (solid line), POL-45 (dashed line) and CHE-45 (dotted line) structures. (Right) Bond angle distributions g(θ) for the BOR-36 sample (a) and the a-120 (solid line), POL-45 (dotted line) and CHE-45 (dashed line) structures (b, c). X1,X2=C,B.

The atomic configurations of the amorphous samples are displayed in Fig. 4. The results presented in Figs. 2–4 show that both amorphous structures are based on a random icosahedral network that does not contain chain atoms. For the a-120 sample a distinct peak associated with the C-C NN correlations suggests clustering of carbon atoms. We also note in Fig. 4 that C-C_1B_2 (A), C-C_4 (B), and C-C_2B_2 (C) configurations are present in this sample. On the contrary, clustering of carbon atoms was not revealed in the a-135 structure. The weak peak associated with C-C NN correlations observed for this structure (cf. Figure 2) is caused by the interactions between the two carbon atoms that are contained in several poly-atomic configurations (cf. Figure 4).

To specify the structural peculiarities of the a-B_4C samples we further analyzed the PCF and the bond angle distribution, g(θ) of the a-120 phase in comparison with those of the crystalline structures. The results are shown in Fig. 5. We see that for the POL-45 structure there are three PCF peaks of the B-C NN correlations related to the correlations in the chain (b1) at ~1.42 Å, between chains and icosahedra (b7) at ~1.60 Å, and inside and between icosahedra (b2, b4, and b6) at ~1.74 Å, cf. Figure 1 and Table II.

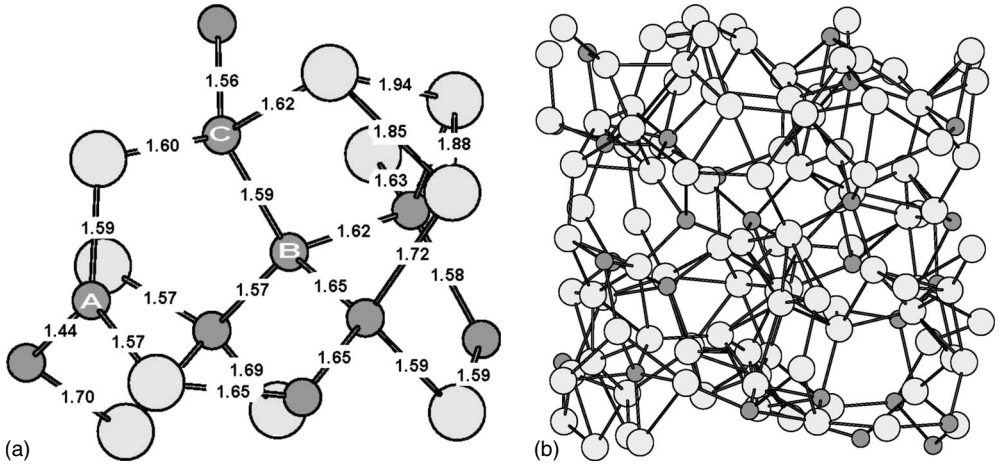

FIG. 4. Fragment of atomic configuration for the a-120 sample with threefold (A) and fourfold (B and C) coordinated carbon atoms (left panel), and atomic configuration of the amorphous 135-atom sample (right panel). Notation: Si atom—large light-gray circle, C atom—small dark-gray circle. Numbers refer to bond lengths.

The C-C NN correlations are missing in this structure, whereas they are present in the CHE-45 structure as indicated by the PCF peak located at ~1.33 Å. The a-120 sample does not have any correlations related to C-C-C or C-B-C chains, and instead shows correlations between carbon atoms in the C-C_1B_2, C-C_4 and C-C_2B_2 configurations, cf. Figure 4. Such correlations are shown in the PCF with a peak at ~1.57 Å and a shoulder around 1.44 Å, which indicates that carbon clusters have different configurations. The wide peak associated with the B-B NN correlation and its location points to the presence of the disordered icosahedra mainly occupied by boron atoms.

This picture of the interatomic correlations is consistent with the bond angle distribution $g(\theta)$ for the crystalline phases and the a-120 sample, shown in Fig. 5 (right panel). For the c-B_4C, the $g(\theta)$ function has three main peaks at 60°, 108°, and 122°. The first two peaks are caused by bond angles within icosahedra, whereas bond angles between icosahedra lead to a third peak, cf. Figure 1. Obviously the angles between the bonds inside the linear chains correspond to 180°.

In the case of a-120, the $g_B(\theta)$ distribution (X1-B-X2,X1,X2=C,B) is broad, but on the other hand, it resembles the corresponding functions for the BOR-36, which indicates that the amorphous sample is mostly composed of distorted boron icosahedra. The broadening of the second peak of the $g_B(\theta)$ distribution can be also caused by the presence of C atoms inside the icosahedra. The $g_B(\theta)$ function does not have a peak around 180° since boron atoms do not occupy the linear chains. The bond angle distribution of carbon atoms in a-120 strongly differs from that in c-B_4C. In particular, the new additional peaks at 80° and 135° arise in the amorphous sample. These peaks are related to the new threefold and fourfold bonds that form with the participation of carbon. As in the case of boron atoms, we do not find any evidence of the formation of linear chains with the participation of carbon atoms. A small peak at 175° in the $g_C(\theta)$ function (X1-C-X2,X1,X2=C,B) (cf. Figure 5) is caused by the angles between the bonds that are formed by the fourfold coordinated carbons. Further inspection of the atomic configuration shows that the carbon clustering cannot be identified as graphitelike or diamondlike, but instead can occur because of the fragments described above. As for the a-135 sample, we carried out a similar investigation of its PCF and $g_C(\theta)$, and did not find any carbon clustering ($g_{C-C-C}=0$). However, for both amorphous samples, the structural parameters (not shown here) are similar.

To compare the experimental and theoretical amorphous structures of a-B_4C we have calculated the vibrational density of states (VDOS) for the a-120 and a-135 samples from the Fourier transform of the velocity autocorrelation function. The description of this computational procedure can be find elsewhere.[33] The calculated VDOSs together with the Raman spectra of the a-B_4C samples derived from crystalline counterparts by indentation (bulk)[10] and prepared in the view of films (film)[21] are presented in Fig. 6. The Raman spectra have been measured at room temperature. The Raman spectrum of the bulk samples are characterized by the two-peak band around 500 cm^{-1} that is assigned to the C-B-C vibrations. The modes in the range 600–1200 cm^{-1} are mainly related to internal vibrations of the icosahedra. The graphitic D and G bands are centered around 1330 and 1500 cm^{-1}, respectively. Finally, a small peak at 1800 cm^{-1} is also shown. In the experimental spectrum of the a-B_4C films we observe only the broad peaks related to internal vibrations of the icosahedra. In the calculated VDOSs, the peaks at 500 and 1800 cm^{-1} are missing. For the a-120 sample, the availability of two bands at 1290 and 1450 cm^{-1} that resemble the D and G bands in the Raman spectrum of the bulk material indicates the formation of carbon clusters. One can see from Fig. 6 that the a-120 and a-135 samples in general terms correctly describe the corresponding amorphous structures of the bulk and film a-B_4C.

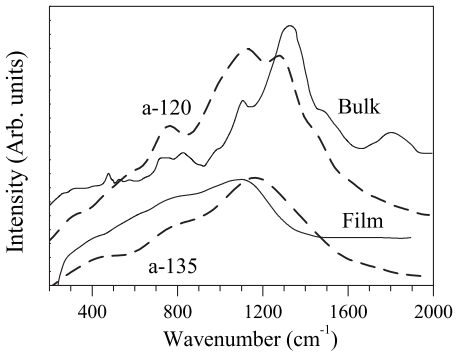

FIG. 6. Comparison of the vibration densities of states of the a-120 and a-135 samples (dashed line) with the Raman spectra of the bulk (Bulk) (Ref. 10) and film (Film) (Ref. 21) materials of a-B_4C (solid line).

In summary, we note that the a-B_4C samples generated from different precursors have different amorphous networks. The sample generated from rhombohedral c-B_4C (a-120) represents disordered icosahedra composed mainly of boron atoms connected by topologically disordered B-C and C-C networks. The sample generated from hypothetical cubic B_4C (a-135) has the structure similar to the one of the a-120 sample, but without carbon fragments. The linear chains that are the characteristic feature of the crystalline structures are missing in both amorphous samples. Most likely, this is the main reason for the decrease in bulk modulus from c-B_4C to a-B_4C, cf. Table I. We also hypothesize that the presence of carbon clusters in the a-120 sample is responsible for an increase in B, when compared to the a-135 sample for which such clusters are missing.

C. Pressure-induced phase transitions

We now examine an effect of pressure on the stability of the crystalline and amorphous samples of B_4C. For this purpose, the total energy of the POL-15, CHE-15, a-120, and a-135 samples was computed as a function of pressure. Figure 7 shows the results of total energy calculations for these samples, and it is worth noting that three phase transitions are predicted as pressure increases (i.e., as cell volume decreases).

To specify the transition pressures and the changes in volume we calculated the enthalpy and the cell volume of these structures as functions of pressure at zero temperature. The

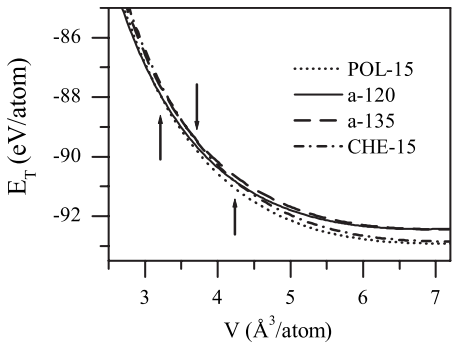

FIG. 7. Total energy (E_T) versus cell volume (V) for the POL-15, CHE-15, a-120 and a-135 structures. The arrows indicate the crossovers of curves.

results of such calculations are shown in Fig. 8. One can see from Fig. 8 (left panel) that the transition pressures for CHE-15 to a-120, CHE-15 to a-135, and POL-15 to a-120 transformations are 300, 530, and 743 GPa, respectively. These phase transformations are accompanied by abrupt volume reductions of 0.18, 0.09, and 0.07 Å^3/atom, respectively, which allows us to identify them as first-order phase transitions (cf. Figure 8, right panel). The total energy curves for the POL-15 and CHE-15 phases do not cross, which does not support the idea that the polar structure can transform into a chain one under pressure.[15] Our results indicate that these structures can transform into their amorphous counterparts only under ultrahigh pressures. Obviously that the transition pressures will be lowered as temperature will increase. Hence, since high pressures and temperatures can be reached under shock loading conditions, such a sample treatment may indeed causes the amorphization of both polar and chain B_4C structures.[7] It is seen that the amorphization of the chain structure occurs prior to the one of the polar structure, cf. Figures 7 and 8.

D. Electronic structure

Here, we focus on the electronic properties of crystalline and amorphous boron carbides. It is known that boron carbide exhibits semiconducting properties.[34] Its band gap (E_g) does not exceed 3.8 eV and depends on stoichiometry.[35] Semiconducting boron carbide is a promising material for true solid-state neutron detection.[36] The optical band gap was found to be reduced to 0.7 eV in amorphous boron carbide.[37]

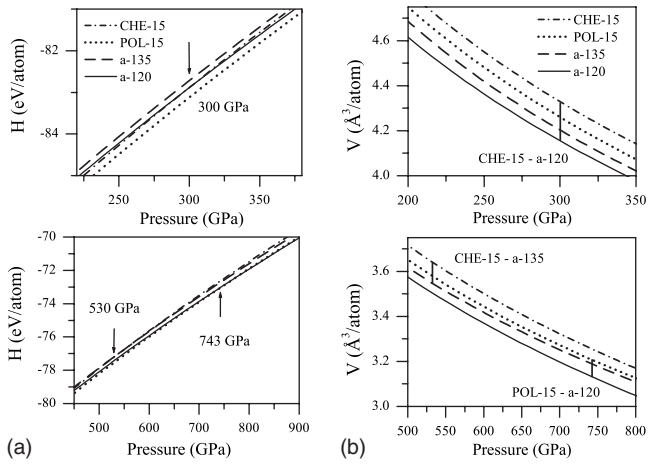

FIG. 8. Enthalpy (H) (left panel) and cell volume (V) (right panel) as functions of pressure for crystalline and amorphous structures.

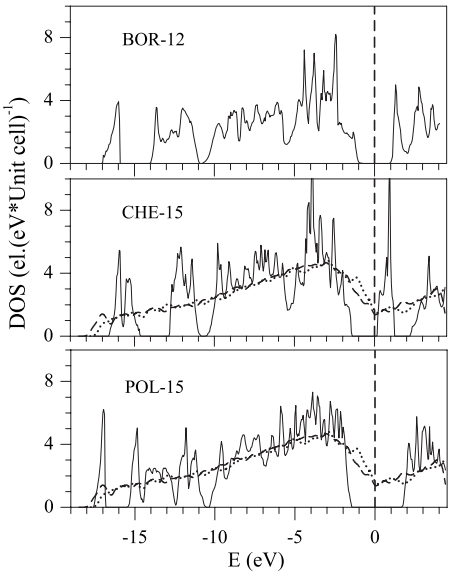

FIG. 9. Densities of states (DOS) of BOR-12, CHE-15 and POL-15, with comparison between the results for a-120 (dotted line) and a-135 (dashed line) supercells. Vertical lines denote the Fermi level.

In Fig. 9, we compare the computed densities of states of crystalline and amorphous B_4C. The results show that the band gaps in the POL-15, CHE-15, and BOR-12 structures are equal to 2.95, 1.55, and 1.83 eV, respectively. We note that the introduction of C-B-C chains in the rhombohedral boron structure leads to a widening of E_g, whereas the existence of C-C-C chains causes a narrowing of the band gap. For the crystalline structures, one peculiarity should be pointed out: the substitution of a boron atom by a carbon atom in the chain leads to the appearance of a narrow band ($\sim$1 eV) in the middle of the wide energy gap ($\sim$3.7 eV). As was mentioned above, in boron carbides there is not a single unit cell representing the whole structure like in common crystalline solids. In practice, the polar B_4C samples can have a small number of C-C-C chains. In this case, the narrow empty band just above the Fermi level will be formed, thereby determining the *p*-type semiconducting behavior of such samples as observed in experiment.[34]

The electronic spectra of the a-120 and a-135 samples are broad because of the disordered amorphous structure. In the amorphous samples the band gap transforms into a broad DOS minimum, cf. Figure 9. Both electronic spectra of a-B_4C are similar. A thorough analysis of the electronic spectra of the amorphous samples shows that the carbon segregation in the a-120 sample gives rise to the broad peak in the region of the DOS minimum. The fact that this broad peak coincides with the distinct peak in the middle of the band gap of the CHE-15 structure speaks in favor of this conclusion, cf. Figure 9. At first glance, the amorphous samples have to show semi-metal properties because of the gap states. How-

ever, we expect that these states to be localized, with the result that our amorphous structures could show slightly semiconducting properties. These properties could be enhanced with an "improvement" in the amorphous network by, for example, annealing, or hydrogen passivation of the dangling bonds. It is worth noting that a weakening of the semiconducting properties of boron carbides during amorphization was noted in Ref. 37.

IV. CONCLUSIONS

We performed first-principles band-structure calculations of the crystalline polar (B_{11}C-C-B-C) and chain (B_{12}C-C-C) structures of B_4C to clarify their geometry. It was shown that only chain structures have hexagonal symmetry. The polar structure undergoes small distortions causing its triclinic symmetry. We have singled out two kinds of amorphous structures of B_4C that include the bulk amorphous phases derived from the crystalline counterparts by mechanical treatment, and the amorphous films deposited from homogeneous gas mixture. To reproduce this experimental situation we have carried out MD simulations on amorphous B_4C samples generated from the crystalline polar cell (a-120 sample, that models the bulk materials) and the cubic fcc cell that does not have common features with the structure of c-B_4C (a-135 sample, that models the amorphous films). The theoretical samples were found to be composed of disordered icosahedra that are connected by an amorphous B-C matrix. In the case of the a-120 structure, the amorphous matrix contains small carbon fragments. Both theoretical samples do not contain linear chains. In a broad sense, these theoretical models realistically describe the peculiarities of the amorphous structures observed in experiment. It was shown that the bulk modulus of a-B_4C is lower than that of c-B_4C because of the missing linear chains. Our results predict first-order phase transitions from the crystalline to amorphous phases under high pressure. The electronic spectra of the theoretical amorphous samples show a DOS minimum instead of a band gap, and therefore should exhibit semimetallic properties. Finally, we hypothesize that the *p*-type semiconducting properties of c-B_4C can be caused by the substitution of boron atoms by carbon atoms in the linear chains.

ACKNOWLEDGMENTS

This work was supported by the STCU under Contract No. 4682. The work of P.T. was performed under the auspices of the U. S. Department of Energy by the Lawrence Livermore National Laboratory under Contract No. DE-AC52-07NA27344. The authors thank V. Kulikovskyy for the helpful discussions during the various stages of this work.

*ivash@ipms.kiev.ua

[1] K. A. Schwetz and A. Lipp, *Ullmannn's Encyclopedia of Industrial Chemistry* (Verlag Chemie, Weinheim, 1985), p. 295.
[2] D. R. Tallant, T. L. Aselage, A. N. Campbell, and D. Emin, Phys. Rev. B **40**, 5649 (1989).
[3] R. Lazzari, N. Vast, J. M. Besson, S. Baroni, and A. Dal Corso, Phys. Rev. Lett. **83**, 3230 (1999).
[4] B. Morosin, T. L. Aselage, and F. S. Feigelson, Mater. Res. Soc. Symp. Proc. **97**, 145 (1987).
[5] A. C. Larson, in *Boron-Rich Solids*, edited by D. Emin, T. Aselage, C. L. Beckel, I. A. Howard, and C. Wood, AIP Conf. Proc. No. 140 (AIP, New York, 1986), p. 109.
[6] D. Simeone, C. Mallet, P. Dubusson, G. Baldinozzi, C. Gervais, and J. Maquet, J. Nucl. Mater. **277**, 1 (2000).
[7] M. W. Chen, J. W. McCauley, and K. J. Hemker, Science **299**, 1563 (2003).
[8] V. Domnich, Y. Gogotsi, M. Trenary, and T. Tanaka, Appl. Phys. Lett. **81**, 3783 (2002).
[9] D. Ge, V. Domnich, T. Juliano, E. A. Stach, and Y. Gogotsi, Acta Mater. **52**, 3921 (2004).
[10] X. Q. Yan, W. J. Li, T. Goto, and M. W. Chen, Appl. Phys. Lett. **88**, 131905 (2006).
[11] M. W. Chen and J. W. McCauley, J. Appl. Phys. **100**, 123517 (2006).
[12] D. Ghosh, G. Subhash, C. Huei, and Y. K. Yap, Appl. Phys. Lett. **91**, 061910 (2007).
[13] G. Fanchini, V. Gupta, A. B. Mann, and M. Chhowalla, J. Am. Ceram. Soc. **91**, 2666 (2008).
[14] X. Q. Yan, Z. Tang, L. Zhang, J. J. Guo, C. Q. Jin, Y. Zhang, T. Goto, J. W. McCauley, and M. W. Chen, Phys. Rev. Lett. **102**, 075505 (2009).
[15] G. Fanchini, J. W. McCauley, and M. Chhowalla, Phys. Rev. Lett. **97**, 035502 (2006).
[16] M. A. Tamor and W. C. Vassel, J. Appl. Phys. **76**, 3823 (1994).
[17] A. C. Ferrari and J. Robertson, Phys. Rev. B **61**, 14095 (2000).
[18] K. Shirai, S. Emura, and S. Gonda, J. Appl. Phys. **78**, 3392 (1995).
[19] M. J. Zhou, S. F. Wong, C. W. Ong, and Q. Li, Thin Solid Films **516**, 336 (2007).
[20] L. G. Jacobsohn and M. Nastasi, Surf. Coat. Technol. **200**, 1472 (2005).
[21] V. Kulikovsky, V. Vorlicek, P. Bohac, R. Ctvrtlik, M. Strnyanek, A. Dejneka, and L. Jastrabik, Diamond Related Materials **18**, 27 (2009).
[22] J. E. Lowther, Physica B **322**, 173 (2002).
[23] T. Letsoalo and J. E. Lowther, Physica B **403**, 2760 (2008).
[24] S. Baroni *et al.*, http://www.pwscf.org/.
[25] D. M. Ceperley and B. J. Alder, Phys. Rev. Lett. **45**, 566 (1980).
[26] J. P. Perdew and A. Zunger, Phys. Rev. B **23**, 5048 (1981).
[27] H. J. Monkhorst and J. D. Pack, Phys. Rev. B **13**, 5188 (1976).
[28] M. Parrinello and A. Rahman, Phys. Rev. Lett. **45**, 1196 (1980).
[29] B. Morosin, G. H. Kwei, A. C. Lawson, T. L. Aselage, and D. Emin, J. Alloys Compd. **226**, 121 (1995).
[30] H. Clark and J. Hoard, J. Am. Chem. Soc. **65**, 2115 (1943).
[31] B. Morosin, A. W. Mullendore, D. Emin, and G. A. Slack, AIP Conf. Proc. No. 140 (AIP, New York, 1986), p. 70.

[32] S. P. Dodd, G. A. Saunders, and B. James, J. Mater. Sci. **37**, 2731 (2002).
[33] P. M. Voyles, N. Zotov, S. M. Nakhmanson, D. A. Drabold, J. M. Gibson, M. M. J. Treacy, and P. Keblinski, J. Appl. Phys. **90**, 4437 (2001).
[34] H. Werheit, J. Phys.: Condens. Matter **18**, 10655 (2006).
[35] B. Sylvester, S.-H. Lin, and B. J. Feldman, Solid State Commun. **93**, 969 (1995).
[36] B. W. Robertson, S. Adenwalla, A. Harken, P. Welsch, J. I. Brand, P. A. Dowben, and J. P. Claassen, Appl. Phys. Lett. **80**, 3644 (2002).
[37] B. Todorovic-Markovic, I. Draganic, D. Vasiljevic-Radovic, N. Romcevic, M. Romcevic, M. Dramicanin, and Z. Markovic, Appl. Surf. Sci. **253**, 4029 (2007).